

Supplementary information

Fate of ^{14}C -labeled few-layer graphene in natural soils: competitive roles of ferric oxides

Shipeng Dong, Tingting Wang, Kun Lu, Jian Zhao, Yang Tong, Liang Mao*

* Corresponding Author. E-mail: lmao@nju.edu.cn. Tel: +86-18851139869; Fax:
+86-25- 89680393

26 pages and 15 figures and 3 tables

1. Experimental Section

1.1. Soil treatments

The soil organic matter (SOM) was removed using NaClO at room temperature according to a previous study¹. Briefly, 30 g soil was mixed with 600 mL 1 M NaClO (pH=7), after which the suspension was stirred for 6 h at 25 ± 0.1 °C. The solid phase was separated by centrifugation at 2000 g for 20 min and this treatment was repeated three times. After the last treatment, the precipitate was washed with deionized water (DI water) three times to remove extra salts; it was finally freeze-dried for further use. The procedure removed 73.1% and 54.3% of SOM from BS and RS, respectively.

A portion of RS was treated with dithionite–citrate–bicarbonate (DCB) to remove free ferric oxides. Briefly, 500 mL 0.3 M sodium citrate, 62.5 mL 0.1 M NaHCO₃ and 10 g of sodium dithionite were added into 10 g RS. Then heated in a water bath at 70 °C for 2 h and keep stirring. The solid phase was separated by centrifugation at 2000 g for 20 min and pour off liquid. The precipitate was thoroughly washed twice with 0.1 M NaCl and then washed with DI water 3 times to remove excess salts and it was finally dried at low temperature for further use.

Another portion of RS was treated with Acid ammonium-oxalate digestion (AAO) to remove amorphous ferric oxides. 700 mL 0.2 M (NH₄)₂C₂O₄·H₂O and 535 mL 0.2 M H₂C₂O₄·2H₂O were mixed and then (NH₄)₂C₂O₄·H₂O or H₂C₂O₄·2H₂O was added to adjust the pH of the mixed solution to 3.0 to obtain the buffer solution. Then 500 mL buffer solution was added to 10 g RS, and shaken in dark at 25 ± 0.1 °C for 4 h. The solid phase was separated by centrifugation at 2000 g for 20 min. After centrifugal separation, the residual amorphous oxide in the soil was washed twice with 500 mL 0.1 M NaCl and then washed with DI water 3 times to remove excess salts and it was finally dried at low temperature for further use.

Hydrous ferric oxide (HFO): The hydrous oxides of Fe (HFO) was synthesized by dissolving Fe(NO₃)₃ using 0.01 M HCl and then rapidly adjusting the solution pH to 7.0 using 0.1 M NaOH. Then the suspensions were aged at room temperature for 48 h and then centrifuged at 2000 g for 20 min. Supernatant solutions were discarded after

centrifugation, the precipitate was dialyzed to remove Na⁺ and Cl⁻ following by being freeze-dried. The hydrous oxides were characterized zeta potential for the determination of zero point of charge (ZPC), X-ray diffraction (XRD) analysis (Fig. S2) and the BET surface area was measured as 284.93 m²/g.

1.2. Preparation of leaching solutions

The adsorption of FLG onto the two soils was conducted at natural pH conditions. Considering that the adsorption experiment will be carried out in soil solutions, we firstly measured the pH of the soil leaching solutions during the experiment. 0.4 g (oven-dried mass) soil was added to 40 mL headspace vials (solid-to-water ratio of 10 g/L is consistent with the adsorption experiment) and the vials were shaken in the dark at 25 ± 0.1 °C with a speed of 170 rpm. The obtained supernatant considered as “soil leaching solution” was then obtained prepared by centrifugation at 1200 rpm for 10 min after shaken for 0.5, 1, 2, 6, 12, 24 h, respectively.

1.3. Sedimentation experiment

Two sets of experiments were designed to discuss the sedimentation of FLG during two process, one for the sedimentation of FLG happened in the rotary shaker (process 1) and another for the sedimentation caused by centrifugation (process 2). For process 1, 4.5 mL soil leaching solutions after leaching for various time was added to centrifuge tube. Then 0.5 mL 5 mg/L FLG was added to obtain an initial concentration of 0.5 mg/L. The centrifuge tubes were shaken in the dark at 25 ± 0.1 °C with a speed of 170 rpm and 2 mL supernatant was taken out at each pre-determined interval (0.5, 1, 2, 6, 12, 24 h) to detect the amount of FLG. For process 2, 4.5 mL soil leaching solutions after leaching for various time was mixed with 0.5 mL 5 mg/L FLG to obtain an initial FLG concentration of 0.5 mg/L. The centrifuge tubes were shaken for 3 min and then centrifugated at 1200 rpm for 10 min and take 2 mL supernatant to detect FLG. The sedimentation ratio was calculated as following equation:

$$a = \frac{(C_0 - C_t)V}{C_0V}$$

in which C_0 (mg/L) and C_t (mg/L) are the initial and the final aqueous concentrations of

FLG, respectively. V (L) is the volume of the solution. a is the sedimentation coefficient.

1.4. Adsorption Experiments

The concentrations of FLG in suspensions were measured at intervals from 0 to 24 h. The quantity of FLG that had distributed into solid-phase q_t (mg/g) at time t (h) was obtained based on the following equation:

$$q_t = \frac{(C_0 - C_t)V}{m}$$

in which C_0 (mg/L) and C_t (mg/L) are the initial and the final concentrations of FLG at each reaction period, respectively. V (L) is the volume of the solution and m (g) is the mass of soil.

In this study, pseudo-first-order and pseudo-second-order kinetic models were used to explore the adsorption process of FLG on soils. The pseudo-first-order model is expressed as the following equation:

$$\log(q_e - q_t) = \log q_e - \frac{k_1}{2.303}t$$

in which q_e (mg/g) and q_t (mg/g) were the amount of FLG adsorbed on soils at equilibrium and at the sampling time (t), and k_1 is the pseudo-first-order-rate constant.

The pseudo-second-order model is expressed as the following equation:

$$\frac{t}{q_t} = \frac{1}{k_2 q_e^2} + \frac{1}{q_e}t$$

in which q_e (mg/g) and q_t (mg/g) were the amount of FLG adsorbed on soils at equilibrium and at the sampling time (t), and k_2 is the pseudo-second-rate constant.

Adsorption isotherms were obtained by mixing various amounts of FLG with 0.05 g of soils. The mass of FLG that had distributed into solid-phase q_e (mg/g) at equilibrium was obtained by mass balance using the following equation:

$$q_e = \frac{(C_0 - C_e)V}{m}$$

where C_0 and C_e is the initial and equilibrium concentration of FLG (mg/L). V is the volume of the solution (L) and m (g) is the mass of soil.

To quantify the relationship between q_e and the FLG concentration in the aqueous phase (C_e) at equilibrium, we fit the data to the linear isotherm equation:

$$q_e = k \times C_e$$

where q_e is the amount of adsorbed FLG on the soils (mg/g), C_e is the equilibrium concentration in the solutions (mg/L) and k is the partition coefficient (L/g).

The control treatments in this study were also fitted to a linear isotherm equation:

$$q_c = k_1 \times C_e$$

where q_c is the amount of settled FLG during the control experiments (mg/g), C_e is the equilibrium concentration in the solutions (mg/L) and k_1 shows the settling of aggregated FLG caused by centrifugation process.

1.5. Desorption experiments

The desorption of FLG from soils was further investigated. Briefly, the soils were first loaded with FLG using the same procedure as described in the batch adsorption experiments. After that, the mixture was subjected to centrifugation and 2 mL of the supernatant was withdrawn for FLG analysis. The precipitate was washed with DI water (deionized water) three times, then all the supernatant was removed and replaced with 5 mL of desorption solution. The vials were shaken at $25 \pm 0.1^\circ\text{C}$, 170 rpm for different times. At sampling time, the vials were centrifuged again and the FLG concentration in the supernatants was determined. Additionally, the desorption solution containing NOM and non-ionic surfactant Tween 80 and the ionic surfactant sodium dodecyl sulfate (SDS) were applied to investigate their influences on the desorption of FLG. A control experiment was carried out by replacing the desorption solution with DI water.

2. Results and Discussions

2.1. Characterization of the FLG and soils

The agglomerates and sheets of FLG were shown in SEM and TEM images (Fig. S1A

and B), respectively, indicating that FLG sheets suspended in water were prone to be crumpled and agglomerated after drying, as well its surface was quite irregular, with dense folds on it. The size distribution analysis showed that most graphene sheets (> 90%) ranged from 30 to 80 nm with the maximal peak around 50 nm (Fig. S1D). In addition, AFM showed that the average thickness was around 0.8 nm (Fig. S1E), indicating that they were mainly composed of 3 layers of graphene sheets. Raman spectra (Fig. S1F) showed that typical D-band (1332 cm^{-1}), G-band (1609 cm^{-1}) and 2D-band (2688 cm^{-1}) were observed in FLG. The estimated zero point of charge (ZPC) for the FLG was around 3.5 (Fig. S1 G), indicating the FLG sheets were negatively charged at neutral conditions in the following tests.

Table S1 showed the specifically different physicochemical properties between the RS and BS. The organic matter content in the BS was measured as 53.6 g/kg, which is four times higher than that in RS. However, the content of free iron oxides in the RS is 44.49 g/kg, which is much higher than that of BS. Besides, the clay content and mineral types of the two soils are also different. The clay content of RS is higher and its main clay mineral is kaolinite, while BS has much less clay and the main clay mineral is montmorillonite. Therefore, it is speculated that the soil component may play an important role in the adsorption behavior of FLG, thereby influence the mobility and transport of FLG in soils.

2.2. Role of SOM in FLG adsorption

To explore the effect of organic matter content in soil on the FLG adsorption, the SOM was removed using NaClO according to a previous study.¹ The results showed that the FLG adsorbed on the two soils drastically decreased after the removal of SOM. The k values decreased by 72.4% and 65.7% for BS and RS, respectively (Table S1), indicating that the SOM played an important role in the adsorption process. Zhang et al. found that peat has the potential to adsorb MWCNTs during their contacting with

soil and sediment particles.² Van der Waals attraction and/or hydrophobic interactions may become dominant in this process and thus cause the distribution of FLG to SOM. While the sorption capacity decreased for both tested soil samples (Fig. S5), the distinction on FLG sorption capacity between two soils was still impressive. Thus, SOM content may not be the key factor responsible for the huge difference in the adsorption capacity of FLG on two soils. In addition, although the treatment applied to remove SOM in this study are relatively mild, the soil mineral surfaces might also be altered to some extent,¹ which may lead to the change of its adsorption capacity on FLG.

2.3. Role of aluminosilicate minerals in FLG adsorption

In this study, two typical aluminosilicate minerals (kaolinite and montmorillonite) in BS and RS were used as model sorbents. According to the results of dynamics and thermodynamics experiments (Fig. S6), it was found that the adsorption rates of FLG on both minerals were relatively slow and the sorption capacities were both low. As mentioned above, the surface charge of FLG was negative under their natural pH conditions, and the montmorillonite and kaolinite were also negatively charged at the tested pHs (4.0, 8.0 and 10.0). Therefore, it could be concluded that the low adsorption capacities of the two aluminosilicate minerals towards FLG was ascribed to the strong electrostatic repulsion between them. Thus, the contribution of both aluminosilicate minerals on the FLG adsorption capacity of soil also may not be regarded as principal.

2.4. Desorption of FLG in soils

As shown in Fig. S9, desorption of FLG from RS or BS in water was lower than 1%, indicating the tightened retention of FLG in soil. However, they also possibly penetrate soil layers once their mobility potentially changed in complex circumstance with the presence of NOM or surfactants. Thus we investigated the desorption of FLG in soils with the affecting of NOM and surfactants. As shown in Fig. S9A, B, the selected surfactants exhibited a low desorption capacity for FLG on RS (< 3%), while a certain desorption capacity for FLG adsorbed on BS was obtained (around 15%). Despite its weak desorption for FLG, low SDS concentrations ($\geq 40 \mu\text{M}$) have been found to achieve colloidal stability in graphene dispersions due to its adsorption on the graphene

which provided sufficient electrostatic repulsion between the graphene sheets.³ Besides, Guardia et al. found that nonionic surfactants appear to be more effective in the stabilization of graphene compared to ionic ones.⁴ This may be an explanation for that Tween 80 showed a slightly stronger desorption capacity than SDS in this study. In addition, NOM showed weak desorption capacity for FLG adsorbed on both BS and RS, accounting to only about 6% of the total adsorption (Fig. S9C, D). Overall, surfactants and NOM could only desorb a small portion of adsorbed FLG on soils, indicating that FLG might suffer an irreversible adsorption on two soils, especially red soil. The higher content of ferric oxides in RS than BS offering stronger electrostatic attraction between FLG and soils lead the weaker desorption, consistent with a previous study showing that GO sheets were able to irreversibly interact with goethite.⁵ The formation of FLG-ferric oxides composites with multiple interaction patterns greatly reduced the opportunities for FLG releasing from the soil. Since the close integration of mineral particles in soils, the irreversible heteroaggregation formed by particle to particle configuration (patterns in Fig. 3E) tightly restricted the mobility of FLG. The observed desorption of FLG may be attributed to the loosely associated small FLG sheets that adsorbed on ferric oxides aggregates as pattern 1. Besides, in present study on natural soil, FLG was also able to be adsorbed by various soil components such as SOM (Fig. S5). The long term desorption treatment offered sufficient time for the dissolving of SOM and resuspension of FLG that associated to SOM. However, the resuspended FLG sheet also needed to overcome the structural hindrance of soil, as has been reported that the high roughness of collector surfaces could enhance the retention of colloids in a column study.⁶ Thus, the desorption potential of FLG mainly relied on their distribution on various components and position in natural soils, which directly determined the mobility of FLG. We thus further performed column transport experiments with natural soils and ferric oxides as filler to investigate the mobility of FLG.

3. Supplementary Figures

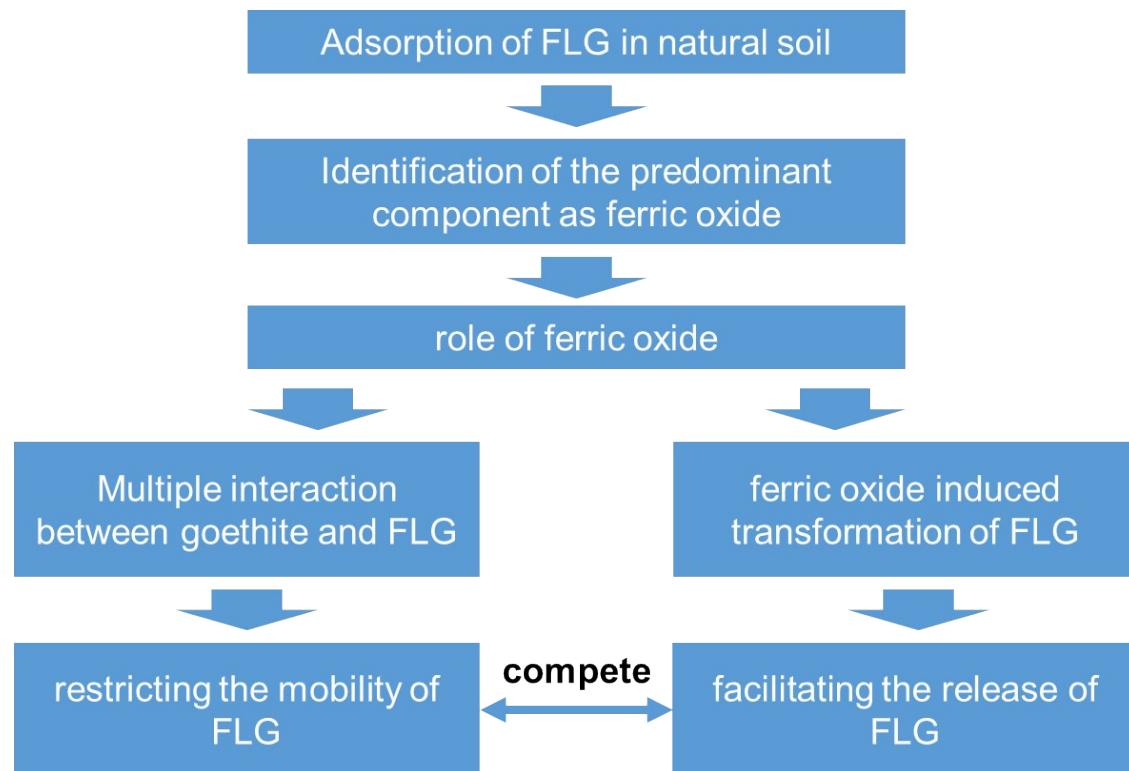


Fig S1 A scheme of the main content of this article

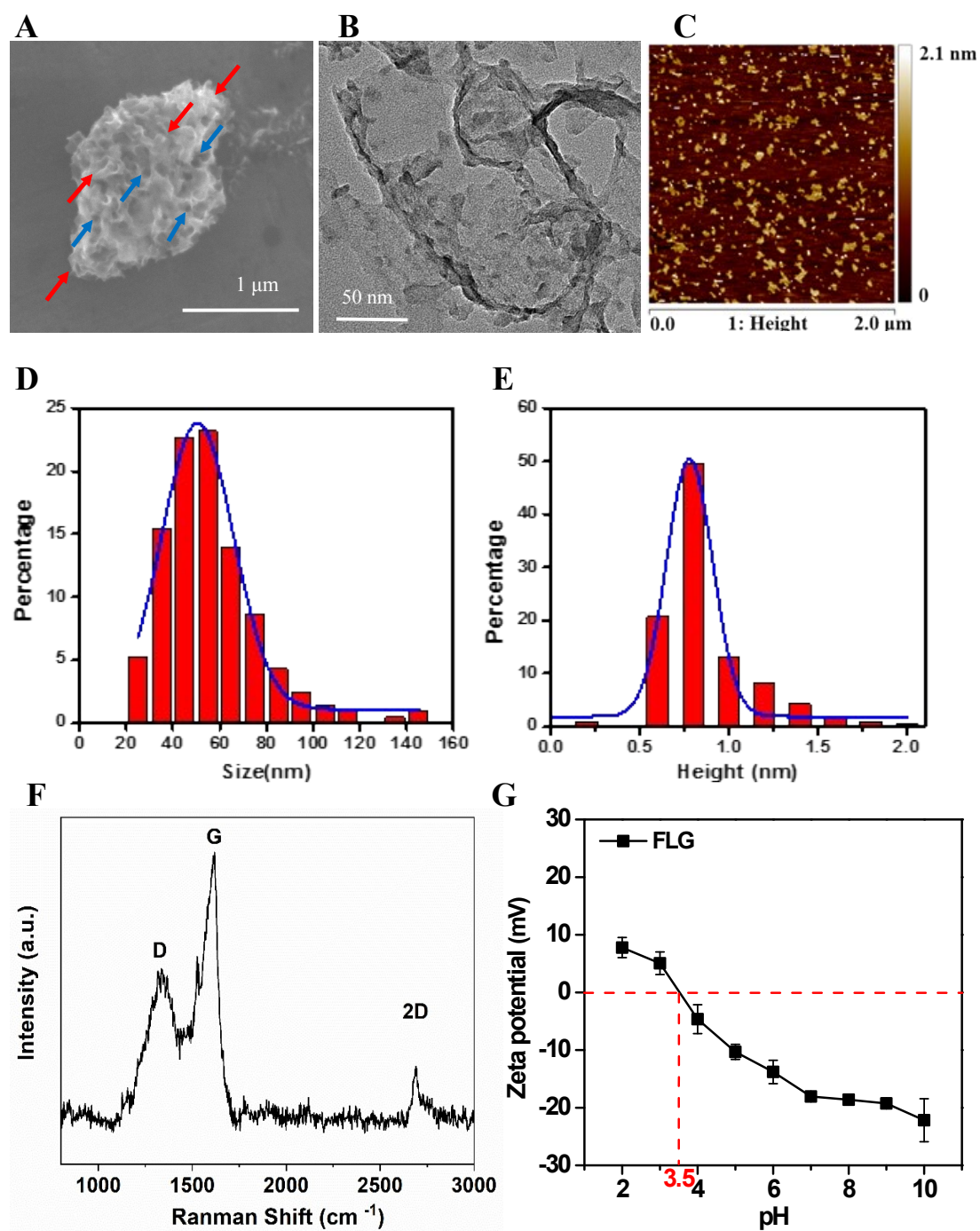


Fig. S2. Characterization of FLG. (A) SEM image. (B) TEM image. (C) AFM image. (D) Histogram of FLG size distribution. (E) Histogram of FLG thickness distribution. (F) Raman spectrum with obvious D and G bands. (G) Zeta potentials of FLG at different pHs.

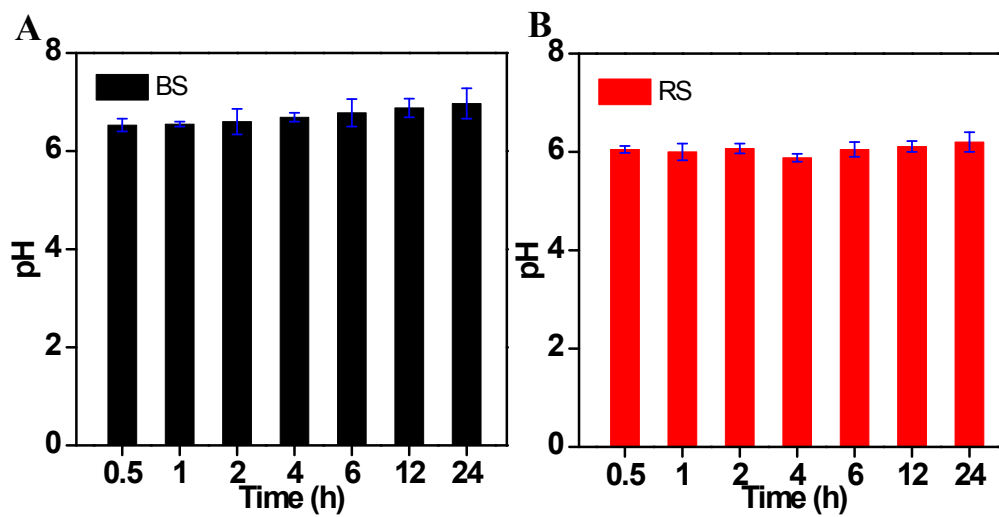


Fig. S3. The pH of soil leaching solutions of (A) BS and (B) RS.

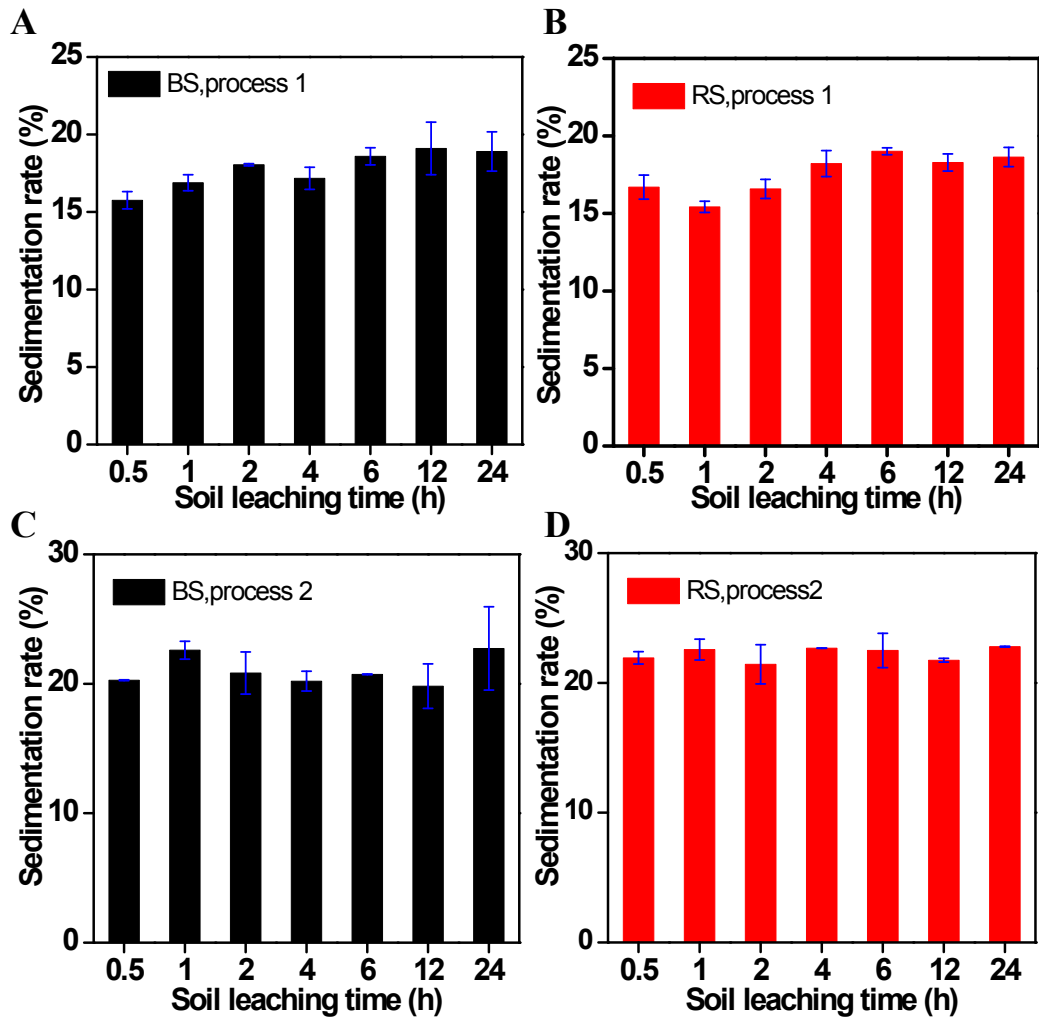


Fig. S4. The sedimentation ratio of FLG in (A) BS and (B) RS leaching solutions during process 1. The sedimentation ratio of FLG in (C) BS and (D) RS leaching solutions during process 2. (process 1: The sedimentation of FLG happened in the rotary shaker; process 2: the sedimentation caused by centrifugation.)

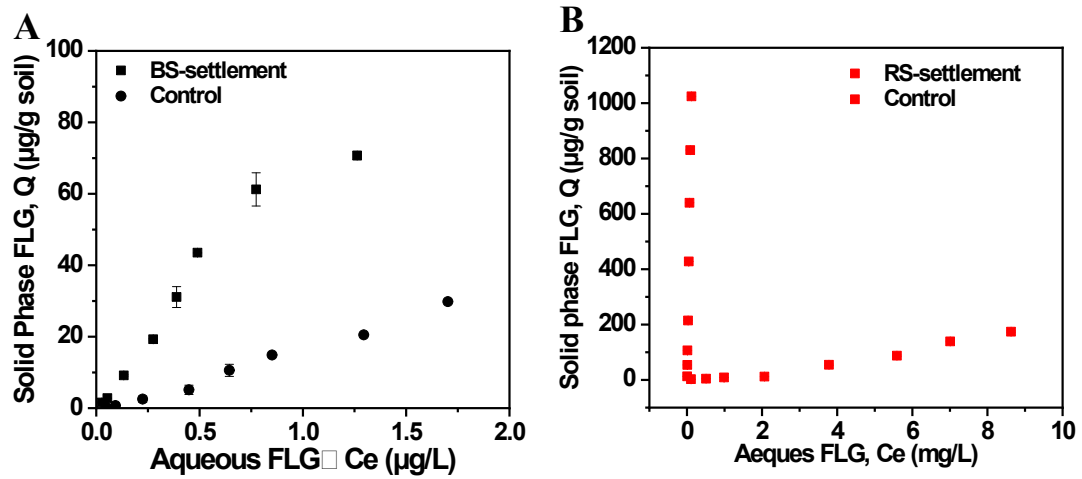


Fig. S5. Settlement of FLG on BS (A) or RS (B) under the natural pH condition

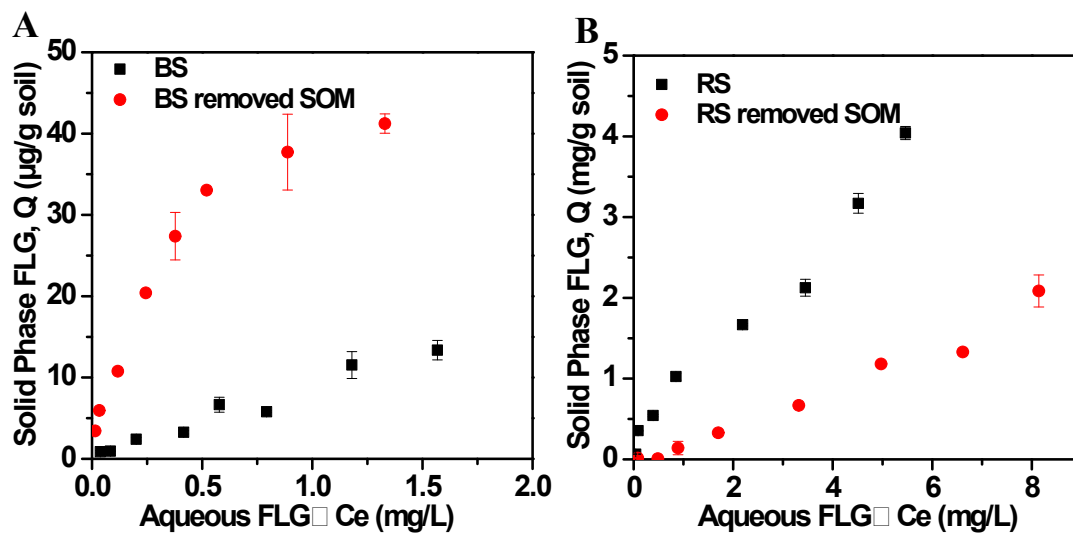


Fig. S6. Adsorption isotherms of FLG on soils and soils removed soil organic matters. (A) BS ([BS]=0.05 g, [FLG]=0.05-2 mg/L). (B) RS ([RS]=0.005 g, [FLG]=0.1-10 mg/L) .

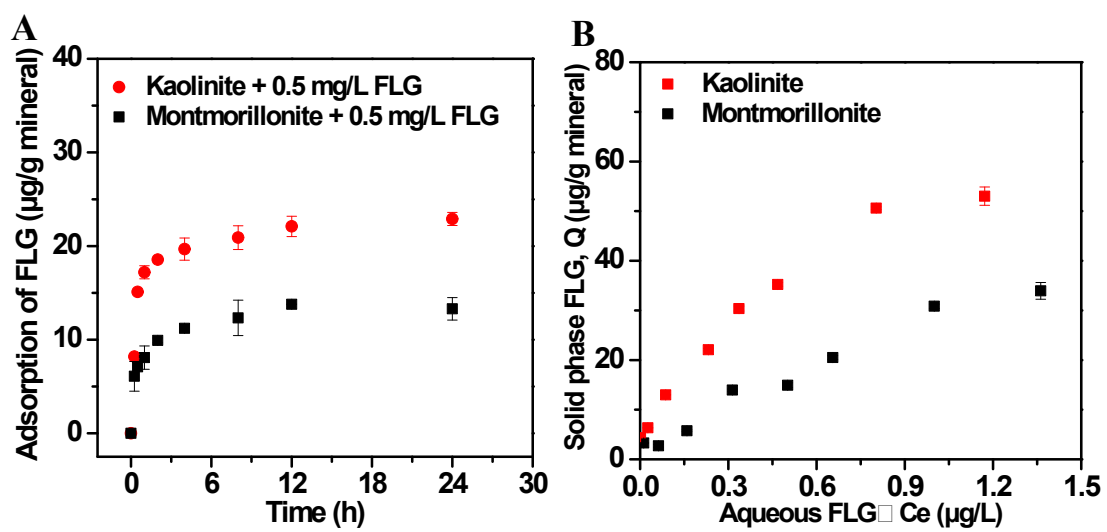


Fig. S7. Adsorption kinetics (A) and adsorption isotherms (B) of FLG on kaolinite and montmorillonite. ($[\text{Minerals}] = 0.05 \text{ g}$, $[\text{FLG}] = 0.05\text{-}2 \text{ mg/L}$)

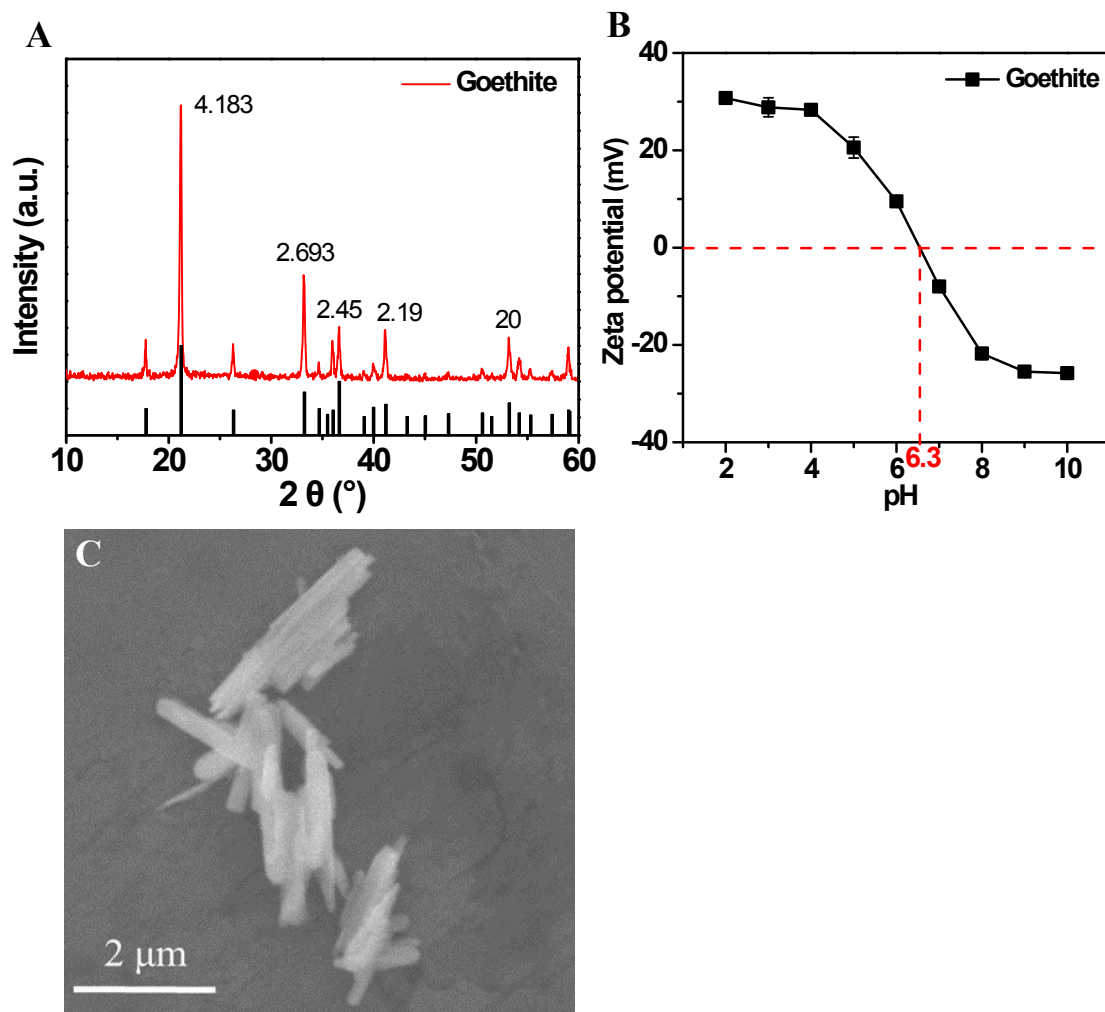


Fig. S8. Characterization of goethite which stood for the crystalline ferric oxides minerals. (A) X-ray diffraction patterns of goethite. (B) Zeta potentials of goethite at different pHs. (C) SEM image of goethite.

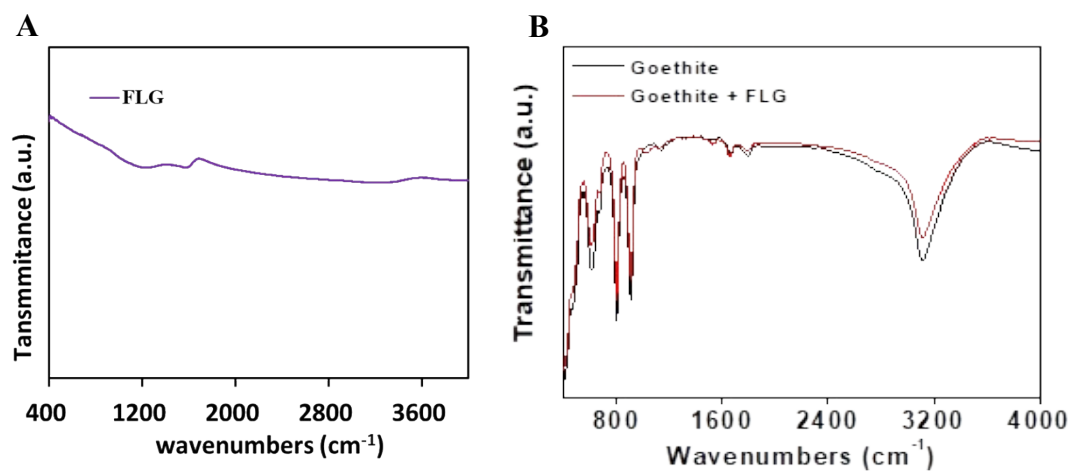


Fig. S9. FTIR spectra of FLG(A) and FLG-goethite complexes(B).

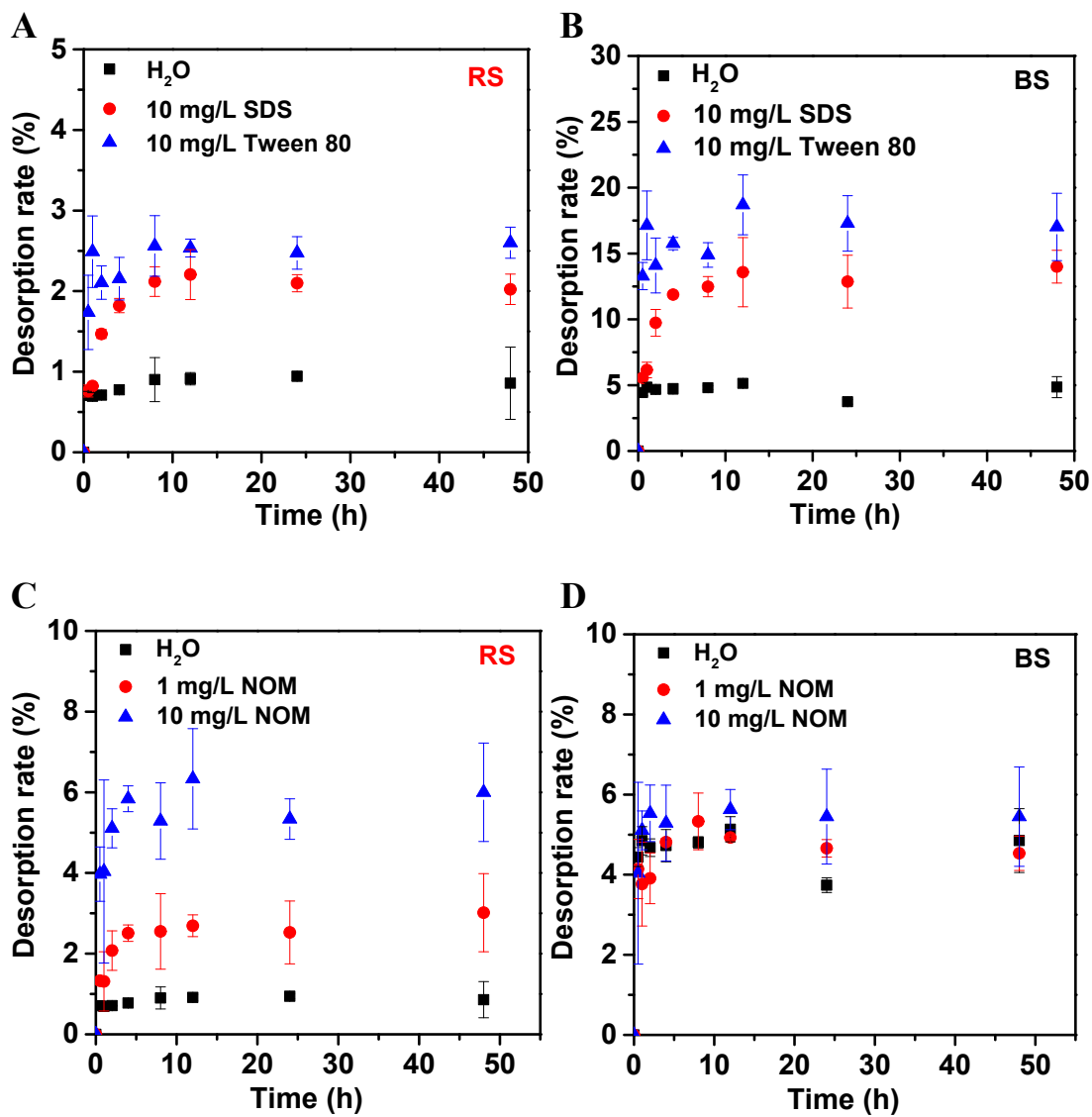


Fig. S10. Desorption kinetics of FLG on (A) RS and (B) BS in the presence of various surfactants. Desorption kinetics of FLG on (C) RS and (D) BS in the presence of NOM.

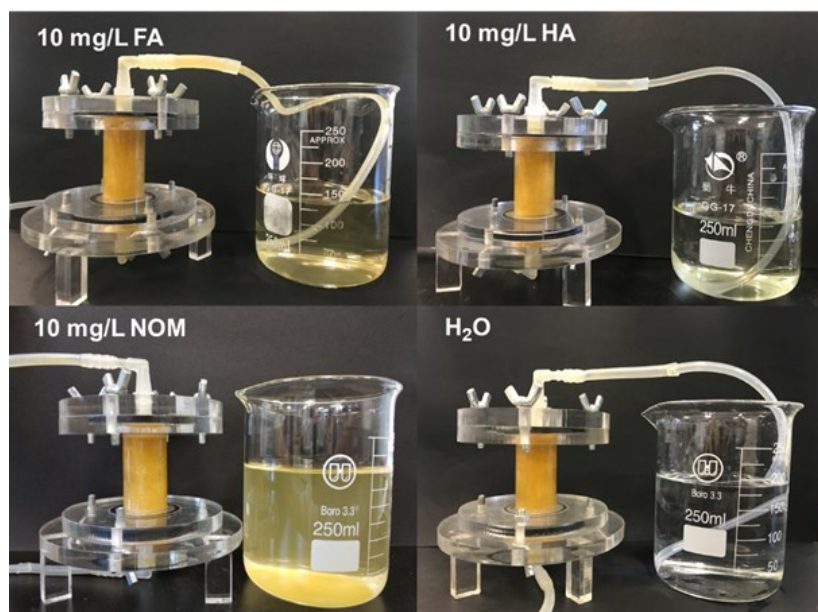


Fig. S11. Photographs of the effluents during the leaching of FLG in the goethite-mixed sand column by NOM, HA, FA and H₂O.

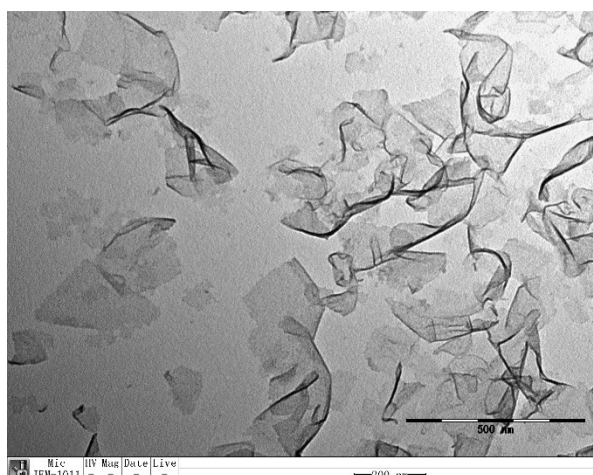


Fig. S12. TEM images of FLG in outflow of goethite filled column after flushing by H_2O_2 solution for up to 21d. The outflow was concentrated by evaporating the solution before the preparation of TEM samples.

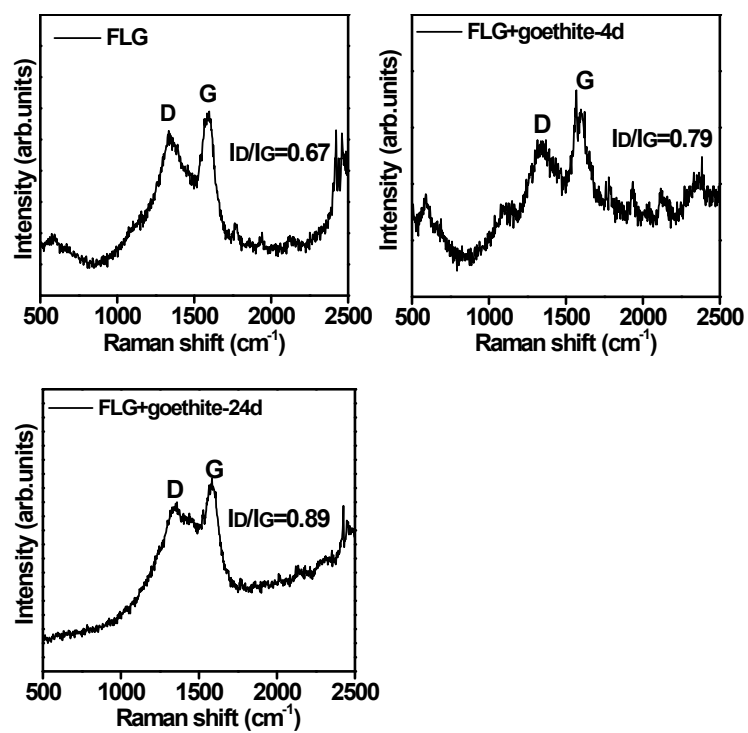


Fig. S13. Raman spectrum of FLG reacted in goethite/H₂O₂ system for different times ([H₂O₂]=20 mM, [Goethite]=100 mg/L). (A) 0 d. (B) 4 d. (C) 24 d.

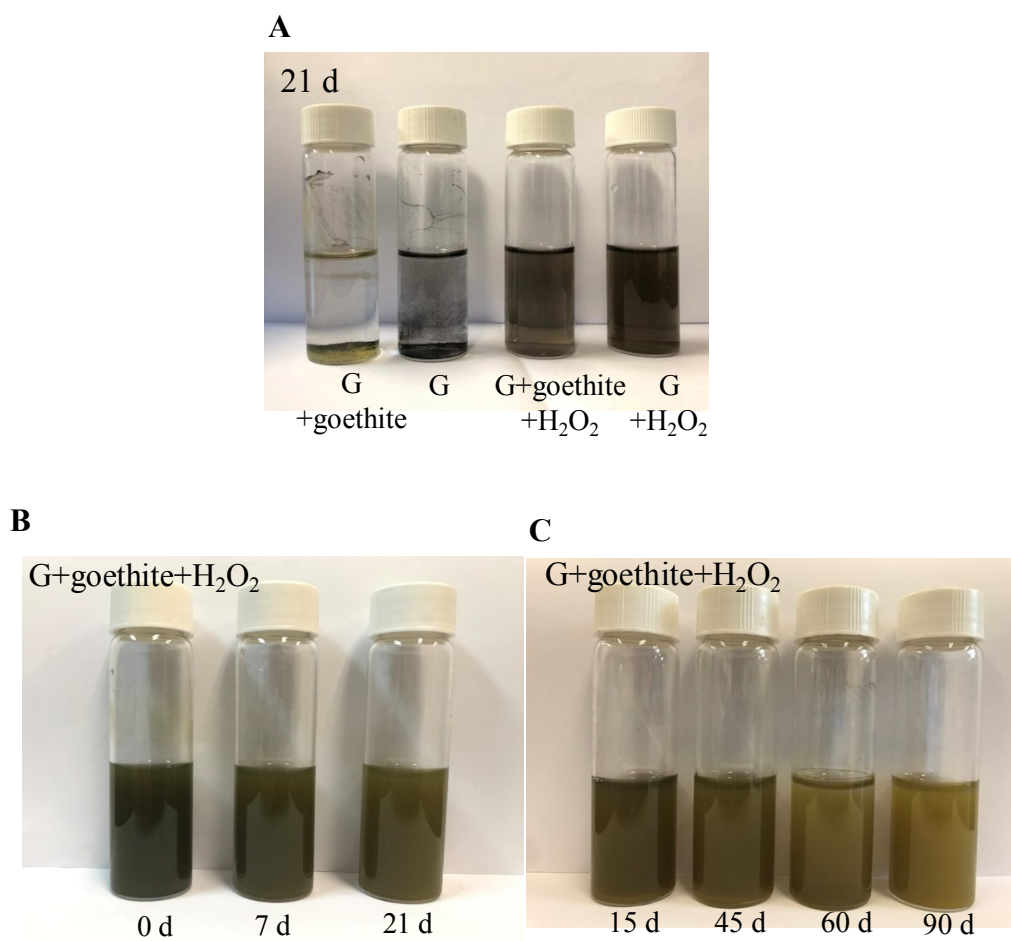


Fig. S14. The degradation of FLG in the goethite/H₂O₂ system. (A) Photograph of FLG in systems variously containing goethite or/and H₂O₂. Photograph of FLG in *the* goethite/H₂O₂ system during (B) short and (C) long times. (G=FLG, pH of the solutions is 4)

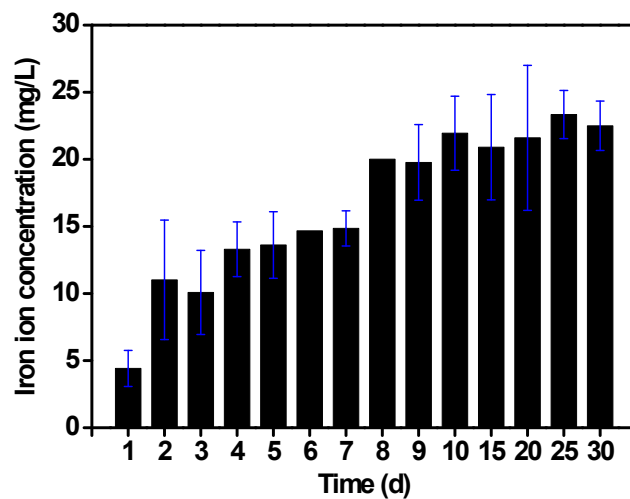


Fig. S15. The concentration of iron ions leached in goethite/H₂O₂ system after reacting for different times.

4. Supplementary Tables

Table S1. Physicochemical properties of two soils in this study.

Sorbents	pH	CEC ^a (cmol/kg)	SOM ^b (g/kg)	DCB Fe ^c (g/kg)	AAO Fe ^d (g/kg)	Surface area ^e (m ² /g)	Texture (%)			main clay mineral
							Clay	Silt	Sand	
RS	6.14	9.7	12.4	44.49	2.08	36.2	14.58	77.59	7.83	kaolinite
BS	6.97	18.7	53.6	9.49	2.3	29	1.31	11.25	87.44	montmorillonite

a Measured by Ba²⁺/NH₄⁺ exchange at pH 8.

b Measured by dichromate oxidation.

c Determined using the DCB digestion method.

d Acid ammonium-oxalate digestion in the dark.

e Measured by N₂-BET method.

Table S2. Parameters of adsorption kinetics equation.

BS Initial concentration (mg/L)	Pseudo-first-order			Pseudo-second-order			RS Initial concentration (mg/L)	Pseudo-first-order			Pseudo-second-order		
	k ₁ (1/h)	q _e (μg/g)	R ²	k ₂ (1/h)	q _e (μg/g)	R ²		k ₁ (1/h)	q _e (μg/g)	R ²	k ₂ (1/h)	q _e (μg/g)	R ²
0.1	1.58	4.39	0.95	0.67	4.54	0.99	0.5	1.38	46.35	0.98	0.04	49.81	0.99
0.25	1.75	8.59	0.86	0.25	9.32	0.94	1	1.81	87.64	0.94	0.026	94.7	0.97
0.5	1.49	19.88	0.95	0.14	20.63	0.98	5	2	459.5	0.99	0.006	487.7	0.99

Table S3. Fitting results of the adsorption isotherms of FLG on soils and minerals by

Linear model.		
Adsorbents (0.05g)	k (L/g)	R ²
BS	0.029±0.15	0.83
BS ₁	0.008±0.21	0.96
RS	7.729±0.02	0.99
RS ₁	0.248±0.23	0.99
RS ₂	0.004±0	0.94
Kaolinite	0.045±0	0.91
Montmorillonite	0.024±0.01	0.97
Adsorbents (0.005g)	k (L/g)	R ²
RS	0.718±0.01	0.95
RS ₃	0.246±0.06	0.98
Adsorbents (0.0025g)	k (L/g)	R ²
HFO	1.460±0.25	0.95
Goethite	15.091±0.47	0.97

BS=Black soil.

BS₁=Black soil removed soil organic matters.

RS=Red soil.

RS₁= Red soil removed amorphous ferric oxides.

RS₂= Red soil removed free ferric oxides.

RS₃= Red soil removed soil organic matters.

References

1. K. Kaiser and G. Guggenberger, Mineral surfaces and soil organic matter, *Eur. J. Soil Sci.*, 2003, **54**, 219-236.
2. L. Zhang, E. J. Petersen and Q. Huang, Phase distribution of ¹⁴C-labeled

multiwalled carbon nanotubes in aqueous systems containing model solids:

Peat, *Environ. Sci. Technol.*, 2011, **45**, 1356-1362.

3. A. G. Hsieh, S. Korkut, C. Punckt and I. A. Aksay, Dispersion stability of functionalized graphene in aqueous sodium dodecyl sulfate solutions, *Langmuir*, 2013, **29**, 14831-14838.
4. L. Guardia, M. J. Fernández-Merino, J. I. Paredes, P. Solís-Fernández, S. Villar-Rodil, A. Martínez-Alonso and J. M. D. Tascón, High-throughput production of pristine graphene in an aqueous dispersion assisted by non-ionic surfactants, *Carbon*, 2011, **49**, 1653-1662.
5. J. Zhao, F. Liu, Z. Wang, X. Cao and B. Xing, Heteroaggregation of graphene oxide with minerals in aqueous phase, *Environ. Sci. Technol.*, 2015, **49**, 2849-2857.
6. C. Y. Shen, B. G. Li, C. Wang, Y. F. Huang and Y. Jin, Surface roughness effect on deposition of nano- and micro-sized colloids in saturated columns at different solution ionic strengths, *Vadose Zone J.*, 2011, **10**, 1071-1081.